Available free online at www.medjchem.com

Mediterranean Journal of Chemistry

Mediterranean Journal of Chemistry **2023**, 13(3), 228-239

Temperature effect on zinc electrodeposition in choline chloride-urea deep eutectic solvent

Mahamadou Sambo Moutari [1], Kindo Adama [1], Moussa Bougouma [1,*], Fousséni Soma [1], Alassane Sorgho[1], Giuseppina Conti [2], Philippe Leclere [2]

[1] Laboratoire de chimie des matériaux et de l'environnement, Université Norbert ZONGO, UFR/Sciences et Technologies (ST), Avenue Maurice Yaméogo, BP 376 Koudougou, Burkina Faso

[2] Laboratory for Physics of Nanomaterials and Energy (LPNE), University of Mons (UMONS), 20 Place du Parc B 7000 Mons, Belgium

Abstract: Zinc electrochemistry was studied on a glassy carbon electrode in choline chloride-urea at 100°C. The cyclic voltammetry results show that reducing Zn(II) to Zn (0) is an irreversible process controlled by diffusion. The voltammogram recorded on GC shows an anodic peak at 0.9 V and a cathodic peak at -1.18 V, corresponding to the oxidation of Zn and its reduction. The voltammogram shows a loop characteristic of a nucleation and growth phenomenon reflected by slow deposition kinetics. Chronoamperometric analysis confirms that Zn electrodeposition occurs following instantaneous three-dimensional (3D) nucleation and growth phenomenon. The diffusion coefficient determined using the Cottrell model is $1{,}9 \times 10^{-6} cm^2.s^{-1}$. The deposit's surface morphology study by scanning electron microscope shows that they are amorphous at 70°C, whereas between 100°C and 110°C, the deposits are very crystalline. EDX analysis reveals the characteristic peaks of Zinc, highlighting deposits made up of Zinc.

Keywords: Zinc, Electrodeposition, Deep Eutectic Solvents, Nucleation, and Growth,

1- Introduction

Zinc is a non-toxic and cheap metal used as a coating for protection against corrosion [1,2], as a source of energy storage, or in electroanalysis [3]. In addition, Zinc and its alloys are also applied in electronics [4], automotive, aeronautics, astronautics, and d various other fields [5]. This arouses a growing interest in obtaining it as a thin layer by electrodeposition or other physicochemical methods. However, for this purpose, the most commonly used methods for zinc electrodeposition in the literature use aqueous or organic solvents that are expensive and less environmentally friendly [6-7]. Thus, to consider the increasingly restrictive environmental and sustainability requirements, many research organizations are committed to developing new compositions of electrolytic baths or new processes. With this in mind, there is growing interest in using unconventional electrolytic media such as deep eutectic solvents (DES) [8]. The term "deep eutectic solvents'' was introduced in 2003 by Abbott et al. [9], with the choline chloride-urea mixture in a stoichiometric ratio of 1:2. In 2014, Smith et al. [10] generalized DES as systems formed from a eutectic mixture of Lewis or Bronsted acids and bases. These DES have remarkable chemical stability towards water and air and low vapor pressure. Moreover, they are less expensive, biodegradable, biocompatible, and less toxic [10-11].

Thus, to satisfy the environmental requirement, authors have used unconventional electrolytic media, such as deep eutectic solvents (SEP), for zinc electrodeposition [12]. So, Abbott et al.[13] worked on zinc electrodeposition in choline chloride -urea and choline chloride -ethylene glycol mixture using a polycrystalline gold electrode. In particular, the study focused on the influence of the viscosity and conductivity of the eutectic solvent containing the dissolved precursors ($ZnCl_2$) on the deposits' qualities. Vieira et al. and Emanuele et al. [14,15] studied working electrode influence such as glassy carbon, steel, gold, platinum, copper, or zinc on zinc electrochemistry in the two media mentioned above in Abbott et al. works. J Chen et al. [16] used choline chloride-urea-ethylene glycol mixture-based eutectic solvent to study Zn electrodeposition on platinum electrode. Another group, [17] did a comparative study of different zinc precursors' influence on the deposit qualities. The choline chloride-urea-ethylene glycol mixture allowed Zhu et al. [18] to extract zinc from electrical and electronic equipment waste.

**Corresponding author: Moussa Bougouma*
Email address: bmoussaraphael@gmail.com
DOI: http://dx.doi.org/10.13171/mjc02306161653bougouma

Received October 21, 2022
Accepted November 10, 2022
Published June 16, 2023

Xiang et al. [19] demonstrated the influence of water additions in the deep eutectic solvent and zinc precursor mix on the zinc deposits. Yang et al. [20] studied the electrodeposition of Zinc in choline-urea chloride media on a tungsten electrode at 100°C. Chronoamperometric analysis of the transient current density indicates that the deposit is characteristic of instantaneous diffusion controlled by three-dimensional (3D) nucleation and growth. Using a scanning electron microscope, the author showed the effect of temperature on zinc surface morphology, which changes from small particles at 70°C to a hexagonal shape at 100°C. Xie et al. [21] also studied Zn electrodeposition in choline-urea chloride media with a copper electrode at 90°C. Scanning electron microscopy results indicate that at 60°C, Zn has a hexagonal shape, at 70°C a flat polygonal shape, while at 80°C and 90°C, it adopts a multilayered structure. Harati et al. [22] obtained the same result as the previous authors on the molybdenum electrode at 90°C. AL-Esary et al. [23] studied the electrodeposition of Zn at 80°C on a platinum electrode in a choline-ethylene glycol chloride media in the presence of additives to stabilize the zinc in the solution. In this study, the potentiostatic analysis of the transient current density indicates that the deposit is characteristic of a three-dimensional (3 D) nucleation and growth of the progressive type.

In this work carried out in a choline chloride -urea mixture, the bath temperature and the precursor ($ZnCl_2$) concentration influence on the morphology of the deposits was studied. The parameters optimization made it possible to obtain deposits that were characterized by SEM and EDX.

2. Materials and experimental methods

2.1. Reagents and solution preparation

In order to study the electrochemical behavior of Zinc, two reagents were used to prepare the solvent (ChCl-U). First, the choline chloride (ChCl) (Alfa Aesar, 98+%) was purified by recrystallization from absolute ethanol (VWR Chemicals, NORMAPUR), filtered and dried under vacuum and urea (U) (VWR Chemicals, NORMAPUR), all mixed in a molar ratio 1:2. At the start of the measurements, the precursor salt $ZnSO_4.7H_2O$ (VWR Chemicals, NORMAPUR) was weighed and directly added without prior treatment to the mixture of choline chloride ($(CH_3)_3NCH_2CH_2OH(Cl)$) and urea ($(NH_2)_2CO$). Then, the entire solid mixture was heated at 110°C for 2 hours with magnetic stirring in an oil bath until a homogeneous and transparent liquid was obtained by using a hot plate (IKA C-MAG HS7) equipped with a temperature sensor and temperature control device (IKATRO N ETS-D5).

2.2. Experimental methods

Electrochemical experiments were performed using a three-electrode system connected to an Autolab PGSTAT302N potentiostat (Metrohm). The measuring cell that contains the electrolyte is made of glass. Before use, all glassware is cleaned with Milli-Q water and oven-dried. The working electrode is made of glassy carbon (BASi, geometric area = 0.0707 cm^2). It is polished with an alumina suspension (1.0 µm) - water on a porous neoprene mat (Struers), then subjected to two periods of ultrasound lasting 5 minutes and rinsed with Milli-Q water to eliminate all tracks of alumina, to finally be dried with nitrogen. The counter-electrode is a platinum grid of about 3 cm^2 of electrochemically active surface. It is cleaned with a flame using a blowtorch of incandescent flame. A silver wire insulated in a capillary tube containing an electrolyte of a mixture of choline chloride/urea (ChCl-U) in 1:2 molar proportions was used as a pseudo-reference electrode. It was rinsed with water and dried with absorbent paper.

3. Results and Discussion

3.1. Potentiodynamic study of Zinc electrochemical behavior on the glassy carbon electrode.

Figure 1 presents cyclic voltammograms recorded in ChCl-U + 50 mmol $ZnSO_4$.$7H_2O$ on a glassy carbon electrode in a temperature range between 70 and 110°C. Each voltammogram consists of anodic and cathodic peaks. From a general point of view, it is observed that the temperature variation does not influence the shape of the voltammograms obtained. However, two important phenomena should be noted. The first is the anodic peak potential shift in the positive direction, while the cathodic peak position is barely varied. The second is an increase in the intensity of the anodic and cathodic peaks. Electrochemical phenomena are consistent with the decrease in the electrolyte's viscosity due to the temperature increase. This allows matter transport more efficiently, resulting in diffusion and a facilitated reduction.

Temperature plays a vital role in the electrodeposition of Zinc and compounds. To this end, a study was conducted to determine the optimum electrolytic temperature in the bath. Among the parameters involved in the most fundamental measurements are the current efficiency (n (%)) and the energy consumption (E) recorded during the measurements. They are respectively determined by Selvarani et al. [17] relations according to equation 1:

$$n = \frac{m \times z \times F}{q \times M} \times 100 \quad (1)$$

With m: the weighed salt mass, z the exchanged electrons number during the Zn^{2+} reduction, F the Faraday constant, q the charge transferred during the

deposition, and M the $ZnSO_4 .7H_2O$ precursor molar mass of in g/mol dissolved in the solvent [13], according to equation 2:

$$E = \frac{V \times Q}{n} \quad (2)$$

With V: the equilibrium potential, Q: the total charge, and n (%) the current efficiency.

The results obtained are recorded in Table 1. The data analysis in this table reveals that the temperature of 100°C presents low energy consumption with a very high effective current efficiency. This observation agrees with the data published by H. Yang et al. [20] in a study carried out in temperatures between 70 and 115°C. Indeed, these authors had shown that the temperature of 100°C has a better salt dissolution efficiency and lower energy consumption. The temperature of 100°C was selected for the rest of our work.

Table 1. Current efficiency (n (%) values and power consumption (E) at different temperatures.

Température(K)	n(%)	E (kWh/kg)
383	103.4	1.84
373	**99.4**	**1.62**
363	80.2	1.89
353	60.3	2.37
343	40.7	3.34

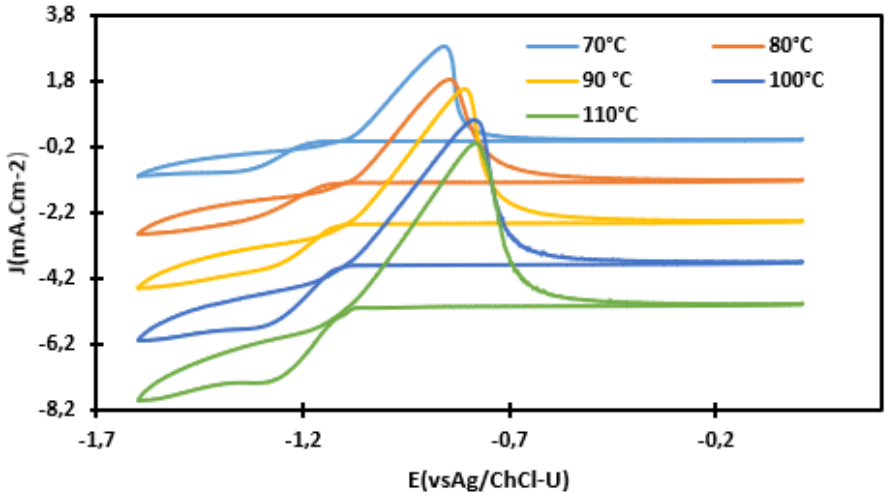

Figure 1. Cyclic voltammogram (3rd cycle) of ChCl-Urea +50 mmol $ZnSO_4.7H_2O$ on glassy carbon electrode at 10mV/s and various temperatures.

Figure 2 below presents cyclic voltammograms (3rd cycle) of ChCl-U + $ZnSO_4.7H_2O$ at various concentrations on the GC electrode. The peak current density curve of the oxidation waves depending on the concentration of ($j = f([Zn^{2+}])$ gives a straight line that passes through the origin of the reference marker (framed in Figure 2).

Thus, the study shows that the anodic current density of the oxidation, waves are proportional to the concentration of the precursor in the solution. Based on these experiments, we can deduce that, apart from the increased current densities of the anodic and catholic waves, the electrochemical behavior of Zn (II) in ChCl-U is not influenced by a concentration variation. In the following steps, all the experiments will be carried out at a concentration of $ZnSO_4.7H_2O$ fixed at 50 mmol.

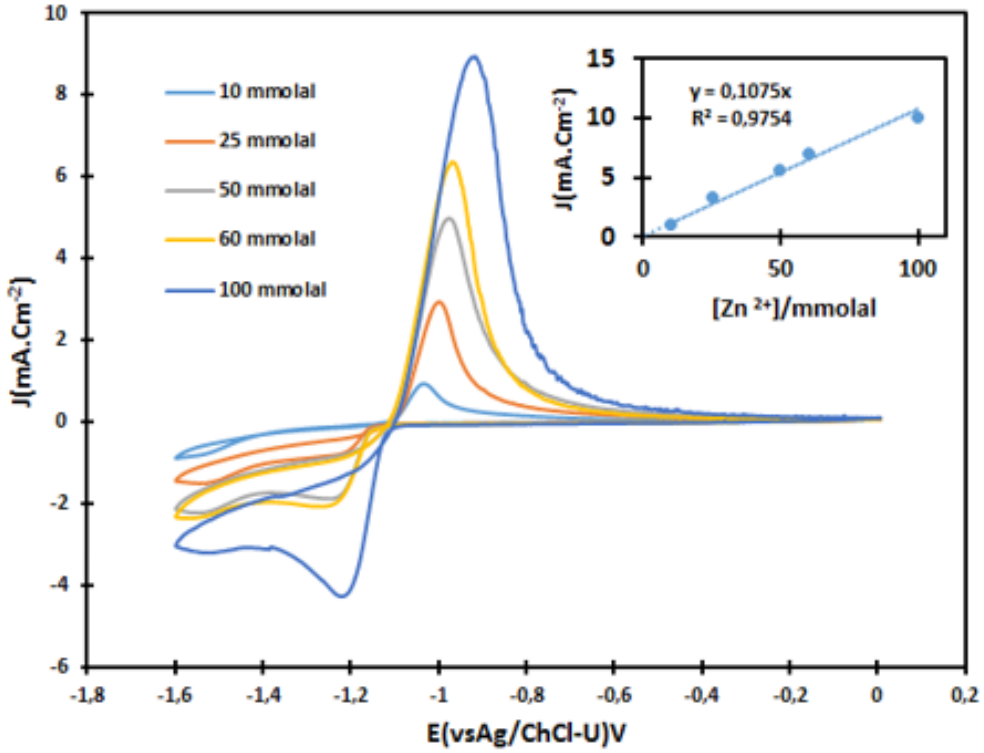

Figure 2. Cyclic voltammograms (3rd cycle) of the ChCl-U system on GC with different concentrations of $ZnSO_4.7H_2O$, v = 10 mV s^{-1}, T = 100°C

Figure 3 shows a cyclic voltammogram at 100°C recorded on a glassy carbon electrode in ChCl-U + 50 mmol of $ZnSO_4.7H_2O$. The Zn(II) species electrochemical response is visible in the GC/ChCl-U accessible window potential. With an experiment carried out in the absence of the zinc precursor (blue curve), it 'is shown that no significant faradic current is observed in the determined window potential. The presence of zinc precursor in the electrolyte presents a reduction (C) and oxidation (A) peaks with the transfer of two electrons, respectively, at potentials of –1.18 V and +0.9V according to the following equations [25] :

Dissolution reaction :

$$ZnSO_4. + Cl^- + urea \rightarrow [ZnSO_4.Cl.urea]^- \quad (3)$$

The cathodic reaction (C):

$$Ch^+ + [ZnSO_4.Cl.urea]^- + 2e^- \rightarrow Zn(s) + [ChCl.SO_4.urea]^{2-} \quad (4)$$

Anodic reaction (A):

$$[ChCl.SO_4.urea]^{2-} \rightarrow Ch^+ + Cl^- + 2e^- + 2O_2 \quad (5)$$

Overall reaction:

$$ZnSO_4 \rightarrow Zn(s) + 2O_2 \quad (6)$$

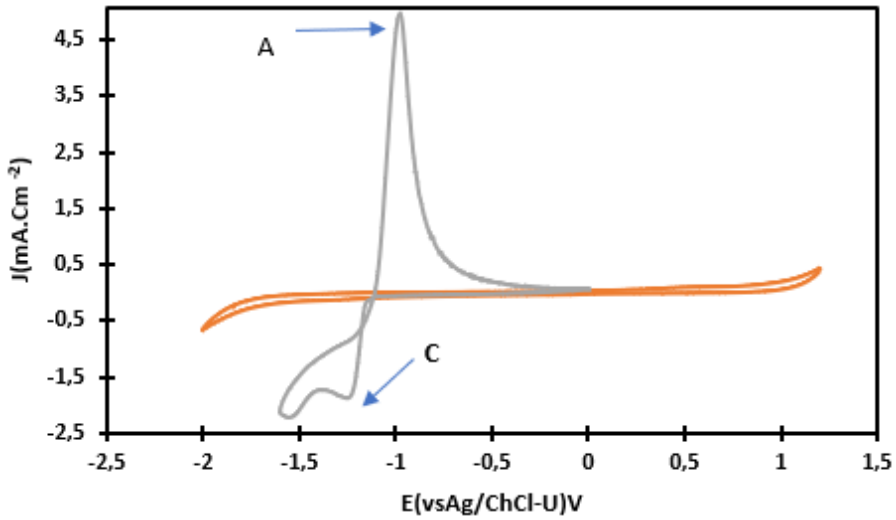

Figure 3. Cyclic voltamperogram of the ChCl-U system + 50 mmol of ZnSO 4.7H_2O, GC electrode, V =10 mV/S, T=100°C.

This result is in agreement with those listed in some other literature references in aqueous [26-30], organic [7,31], ionic liquid [32-35], and deep eutectic solvent media [20, 21].

Figure 4 shows cyclic voltammograms recorded at different sweep rates. Plotting the anodic current density curve against the square root of the scan rate gives a straight line. This electrochemical phenomenon is characteristic of a kinetics reaction controlled by diffusion. In addition, the cathodic peaks are displaced towards negative potentials with the increase of the scan rate. This reflects an irreversible electrochemical process.

The voltammogram in Figure 4 or those in Figures 3, 2, and 1 shows a loop. This phenomenon in electrochemistry is synonymous with nucleation and growth. Yang observed the same phenomenon et al. [20] on a Tungsten electrode in a ChCl-U media.

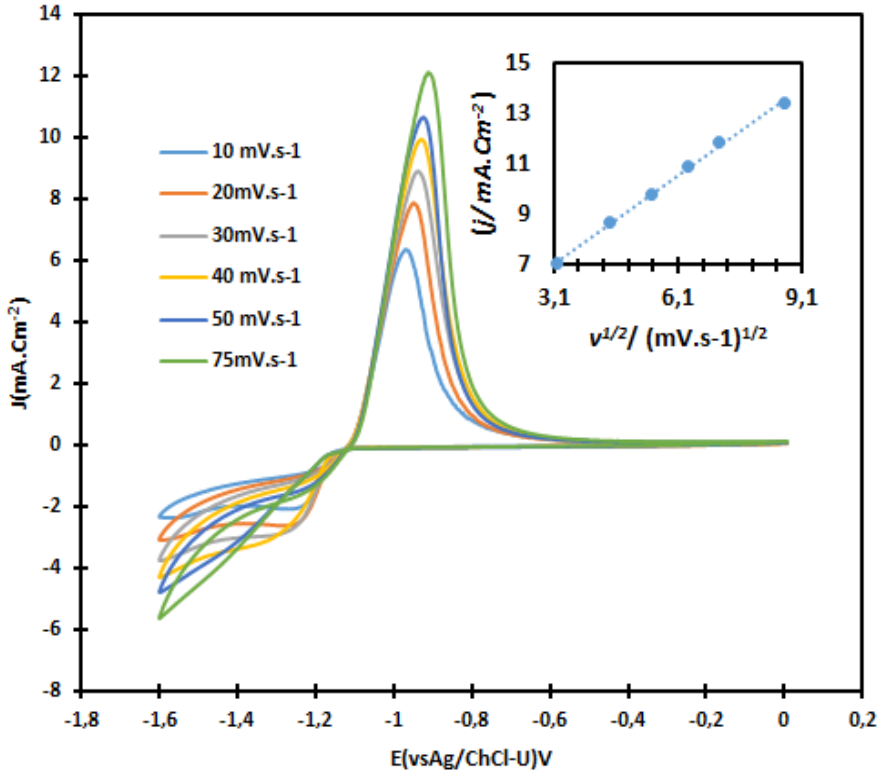

Figure 4. Cyclic voltammograms of ChCl-U + 50 mmol $ZnSO_4.7H_2O$ on GC electrode at different scan rate; T=100°C.

3.2. Potentiostatic study of Zinc electrochemical behavior on the glassy carbon electrode

To better study nucleation and growth phenomenon revealed by voltammetric studies, chronoamperometry measurements were carried out in ChCl-U + 50 mmol $ZnSO_4.7H_2O$ at 100°C on GC. The appearance of transient curves recorded in Figure 5 provides information on the various phenomena at the electrode surface. The glassy carbon electrode is subjected to a potential of 0 V (E1) for 1 s and a second potential of -1.12 V (E2) for 5 s to record these transients. This procedure consists of an electrochemical preparation of the working electrode by eliminating any residual deposits of Zn or other impurities on the electrode surface. This procedure allows the minimization of the residual current linked to the potential jump. Finally, a variable potential (E3) between -1.42 V and -1.46 V is applied to the electrode for 20 s, from which the recording of the deposit phenomenon corresponding to a transient will occur each time. The chronoamperometric analysis of the current density transients (Figure 5) indicates that they go through a maximum at short times when the cathodic potential increases.

At more negative potentials, the transients converge at long times to the behavior described by Cottrell's diffusion equation, according to which the representation of $j = f(t^{-1/2})$ is a straight line, as shown in Figure 6. The slope of the curve $j = f(t^{-1/2})$, denoted "**a**" which is 0.0095, is used to calculate the value of the diffusion coefficient (D0) of the species which diffuse towards the glassy carbon electrode. D_0 is therefore obtained by the method of identification between the Cottrell equation and that of the straight lines with slope "a" according to the following relation of Myland et al. [36]:

$$D_0 = \left(\frac{a}{0{,}564 * n * F * C}\right)^2 \quad (7)$$

With a: the slope of the curve $j = f(t^{-1/2})$, n the number of electrons exchanged during the reduction of Zn^{2+}, F the Faraday constant, and C the concentration of the precursor salt (C (mol.cm^{-3})). The value of the calculated diffusion coefficient is

1.9×10^{-6} $cm^2.s^{-1}$. This coefficient value highlights the rapidity of the electroactive species' mobility toward the electrode substrate surface. Indeed, other authors such as [15,18, 19-22] have found D_0 values lower than ours in the same media with different substrates. Simanavicius et al. [37] estimated the diffusion coefficient of Zn (II) at 1.8 ± 0.2 x 10^{-6} cm^2 s^{-1} in a mixture of aluminum bromide ($AlBr_3$)/dimethyl-ethylphenylammonium bromide (DMEPAB) in a ratio (1:2) on platinum electrode. The value found by Simanavicius et al. is very close to that obtained in this work. However, ionic liquids have a lower viscosity than SEPs [38].

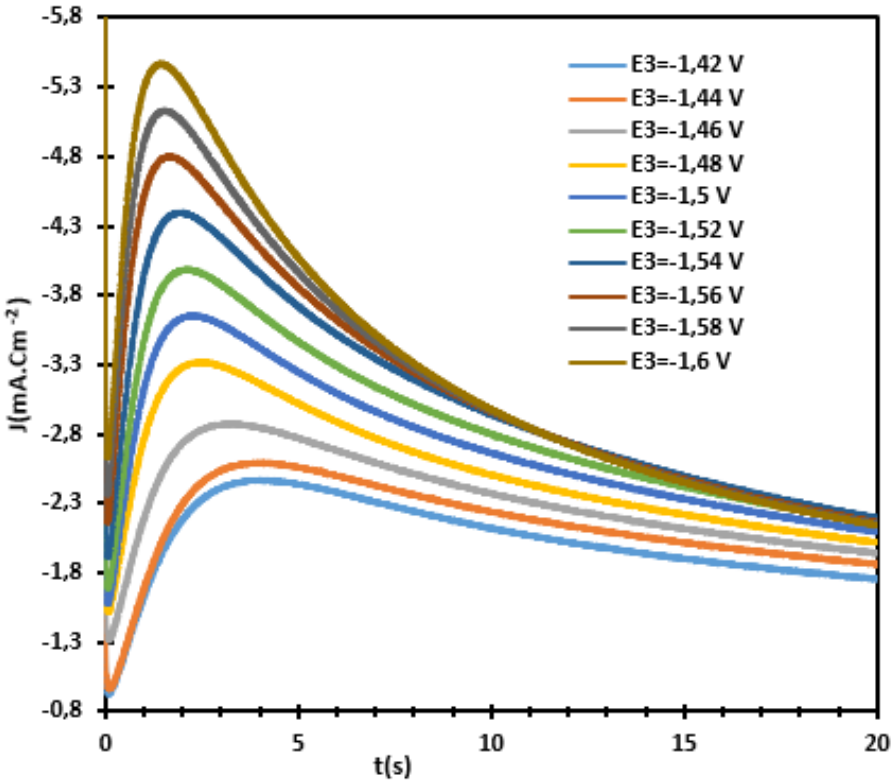

Figure 5. Transients recorded by chronoamperometry in ChCl-U + 50 mmol $ZnSO_4.7H_2O$ on GC, T = 100°C.

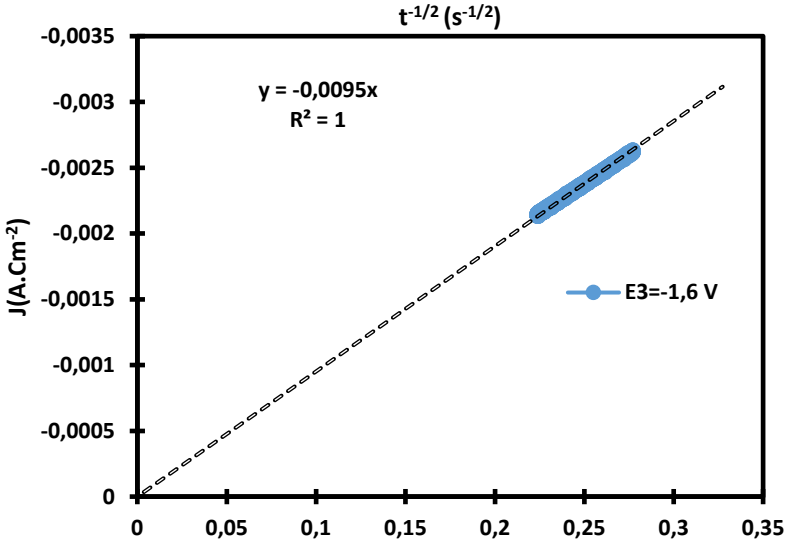

Figure 6. Curves of $j = f(t^{-1/2})$ *in ChCl-U + 50 mmol* $ZnSO_4.7H_2O$ *on GC, T = 100°C.* (E_1=0 V, E_2=-1.12 V, E_3, variable between -1.42V and - 1.6V).

The mechanism of nucleation and growth was studied from the transients recorded by chronoamperometry in Figure 5. For the study, several theoretical models of nucleation and growth are listed in the literature [39-42], but the theoretical models of Scharifker and Hills [39] are used in this work. Figure 7 presents the experimental curves without the dimension of

current density $(\frac{j}{j_m})^2$ as a function of $(\frac{t}{t_m})$ obtained from the exploitation of the transients of Figure 5.

These experimental curves are represented in the same graph as the theoretical curves of Scharifker and Hills relating to instantaneous 3D nucleation (8) and progressive 3D nucleation (9):

$$\left(\frac{j}{j_m}\right)^2 = 1.9542 * \left(\frac{t_m}{t}\right) * \left\{1 - \exp\left[-1{,}2564 * \left(\frac{t}{t_m}\right)\right]\right\}^2 \quad \text{NI (8)}$$

$$\left(\frac{j}{j_m}\right)^2 = 1.2254 * \left(\frac{t_m}{t}\right) * \left\{1 - \exp\left[-2{,}3367 * \left(\frac{t}{t_m}\right)^2\right]\right\}^2 \quad \text{NP (9)}$$

The analyses of the various transient curves in Figure 7 obtained as a function of temperature shows that it considerably influences the zinc electrodeposition. At low temperatures (70°C (a) and 80°C (b)), the transient curves lie between the instantaneous and progressive 3D model curves of Scharifker and Hills. Thus at these temperatures, the mechanism of nucleation is not clearly defined. This phenomenon could be explained by parasitic reactions at the electrode at these temperatures. To this end, Emanuele et al.[15] concluded that the presence of water molecules in the media leads to parasitic reactions at the surface of the electrode during the deposition of Zn. This phenomenon makes the deposits amorphous. At the temperature of 90°C, the experimental curves are close to the instantaneous 3D model curve of Scharifker and Hills. There is a gradual improvement in the deposition mechanism due to the temperature rise. At 100°C, the experimental curves have a good superposition with those of the instantaneous 3D model of Scharifker and Hills. At 110°C, the experimental transient curves move away from the fast 3D model curve of Scharifker and Hills. This could result from the release of ammonia present in the solvent [20].

The study shows that the shapes of the experimental curves (Figure 7 d) follow the theoretical ones of Scharifker and Hills relating to nucleation and three-dimensional (3D) growth of the instantaneous type. This result is confirmed by the slope values from the logarithmic plot of the rising part of the log (-j) transients depending on log (t), which are all close to 1/2 (instantaneous type) (Figure 8).

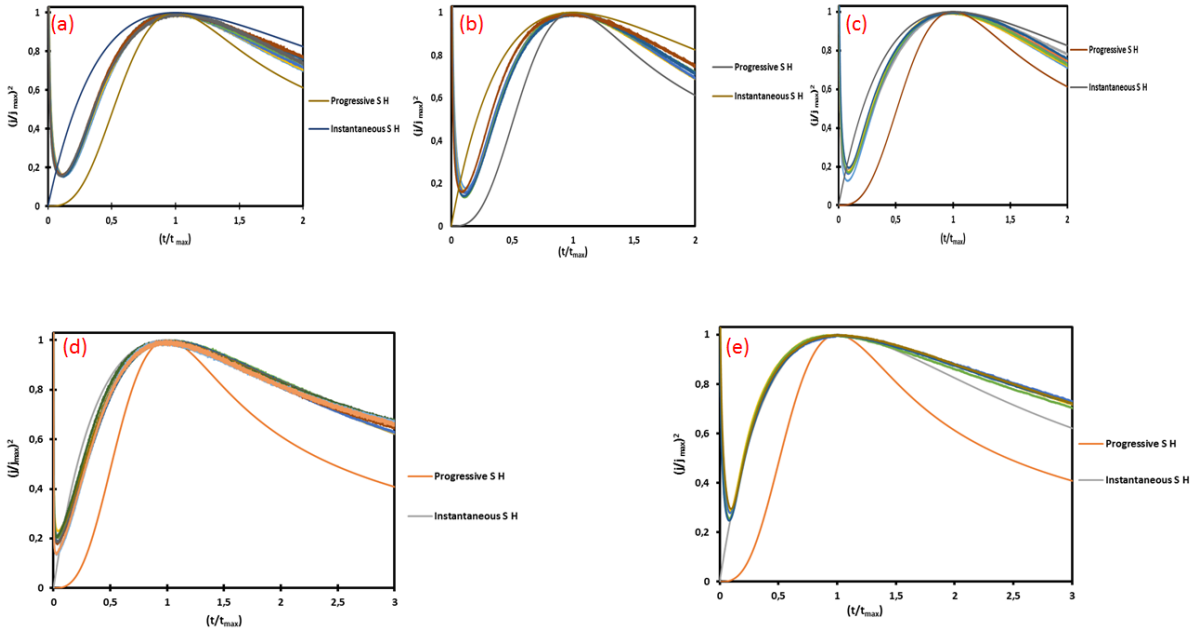

Figure 7. Dimensionless curves $(\frac{j}{j_m})^2 = f(\frac{t}{t_m})$ from current density transients recorded in *ChCl-U* + 50 mmol $ZnSO_4.7H_2O$ *on GC, T = 100°C.*

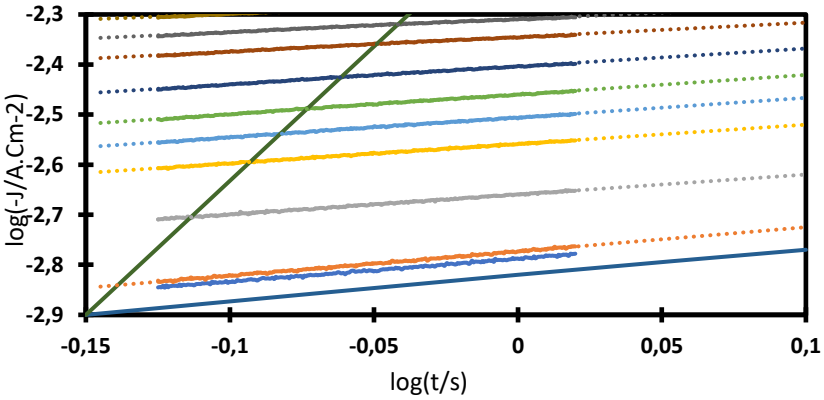

Figure 8. Bilogarithmic plot $\log(-j) = f(log(t))$ of the ascending parts of the dimensional transients: the blue line represents the 1/2 slope (instantaneous type), and the green line represents the 3/2 (progressive type) slope.

Knowledge of electrochemically active sites number on the electrode surface that can easily promote deposition also makes it possible to determine the optimal deposition potential. Thus, after choosing the nucleation mechanism type, it was possible to decide on the number of active sites per unit area N_0 for each applied potential in the limit case of instantaneous nucleation. The N_0 is calculated from the value of the maximum current J_{max} and the maximum time t_{max} according to the following relation of Allongue et al. [43].

$$N_0 = 0.0652 \left(\frac{\rho}{8\pi CM}\right)^{1/2} . \frac{(nFC)^2}{j_m^2 . t_m^2} \qquad (10)$$

With: N_0 the number of sites per active surface unit ($cm^{-2}\ s^{-1}$), n the number of electrons exchanged, F the Faraday constant, C the concentration of the precursor salt (C ($mol.cm^{-3}$)) , M the molar mass of the compound (($ZnSO_4.7H_2O$) = 287.54 $g.mol^{-1}$), ρ the density of the Zinc (ρ (Zn) = 7.14 $g.cm^{-3}$), j_m the density of the current ($A.cm^{-2}$) and t_m the deposition time. The obtained results are recorded in Table 2.

Table 2. Nucleation rates at different applied potentials.

Potentiel appliqué **(E_3)** , V	t_{max}(s)	J_{max}(A/cm^2)	$(t_{max})^2 x (j_{max})^2$ $A^2.s^2.cm^{-4}$	$N_0/cm^{-2}\ s^{-1}$
-1.42 V	4.036	-2.48 x10^{-3}	1 x10^{-4}	1.82 x10^4
-1.44 V	4.08	-2.6 x10^{-3}	1.13x10^{-4}	1.61x10^4
-1 .46 V	3.35	-2.89 x10^{-3}	9.37x10^{-5}	1.9x10^4
-1.48 V	2.48	-3.33 x10^{-3}	6.85 x10^{-5}	2.67 x10^4
-1.5 V	2.23	-3.66 x10^{-3}	6.67 x10^{-5}	2.74 x10^4
-1.52 V	2.16	-3.99 x10^{-3}	7.44 x10^{-5}	2.45 x10^4
-1.54 V	1.88	-4.40 x10^{-3}	6.84x10^{-4}	2.67 x10^4
-1.56 V	1.59	-4.81 x10^{-3}	5.86x10^{-5}	3.12x10^4
-1.58 V	1.55	-5.14 x10^{-3}	6 .31x10^{-5}	2.89 x10^4
-1.6 V	1.42	-5.48 x10^{-3}	6.06 x10^{-5}	3.02 x10^4

The table analysis reveals an increase in (N_0) when the deposition potential tends towards more negative values. Simanavicius et al. [37] studied the nucleation parameters related to the electrodeposition of Zn on a platinum electrode in an ionic liquid media. In our case and that of these authors, the number of sites per unit area (N_0) increases when the deposition potential tends towards more negative values. Our results generally reveal a high density of zinc deposition on the electrode surface. It appears that the deposit will be more considerable at the potential of -1.6 V, which will be taken as the optimal potential for Zinc recovery on the glassy carbon electrode.

3.3. Scanning electron microscopy (SEM) characterization of zinc thin films

Figure 9 presents SEM micrographs of the deposits obtained on carbon substrate at different temperatures. An amorphous and compact layer with a smooth and shiny appearance is observed at 70°C (Figure 9a). However, the micrograph of Figure 9a shows cracks, a sign of the presence of crystals in very

few quantities. The micrograph of Figure 9b (80°C) shows a gradual onset of crystallization by highlighting thin non-uniform layers with small crystallites. At 90°C (Figure 9c), the recorded micrographs show crystallites much more constituted than the micrographs of Figure 9b. The micrographs of Figure 9d recorded at 100°C shows a surface consisting of well-crystallized and dense crystallites with a multilayered structure. At 110°C (Figure 9e), a surface with crystallites is observed with a significant presence of porosities on the deposit's surface, synonymous with the beginning of thin film electrodeposited deterioration. It is, therefore, clear that at low temperatures, thin films have a lower quality with lower crystallinity but which improves with temperature. However, at high temperatures (110°C), the films are well crystallized but deteriorate with the effect of temperature. It appears that the temperature of 100°C allows a well-crystallized surface with less porosity. This confirms the previous results on the choice of this temperature. Thus, the

SEM results agree with those obtained by Yang et al. [20] and Xie et al. [21], who showed the influence of temperature on the electrodeposition of Zinc on tungsten and copper substrates.

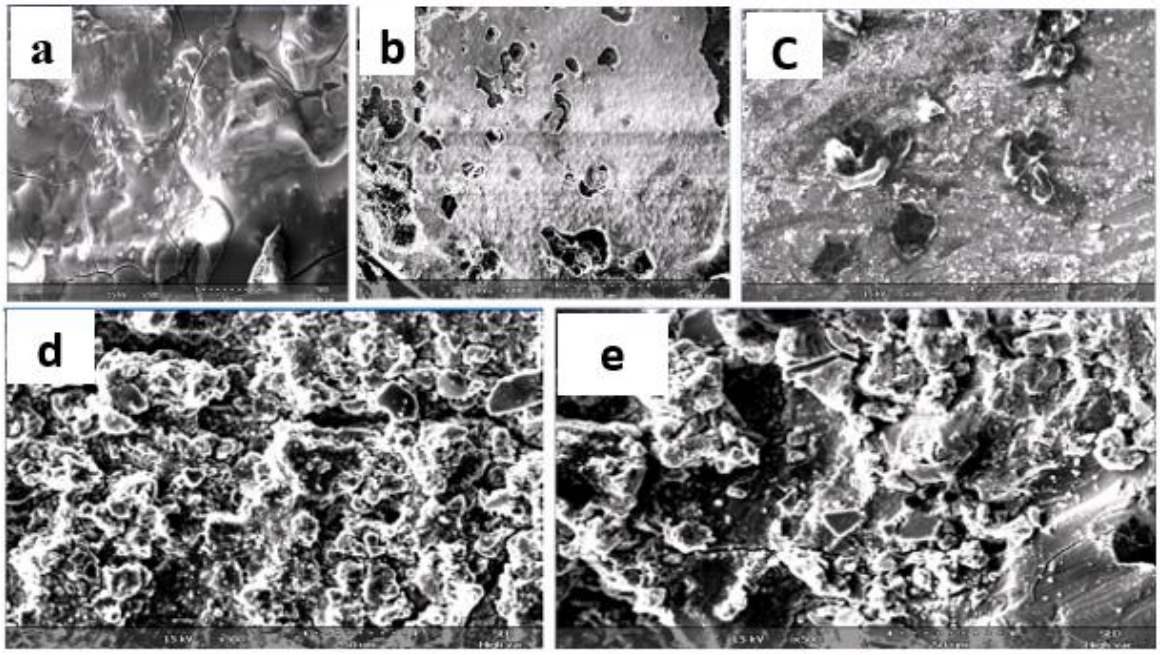

Figure 9. Micrographs of thins films electrodeposited by Scanning Electrons (SEM) : (a) 70°C, (b) 80 °C, (c) 90°C, (d) 100°C, (e) 110°C.

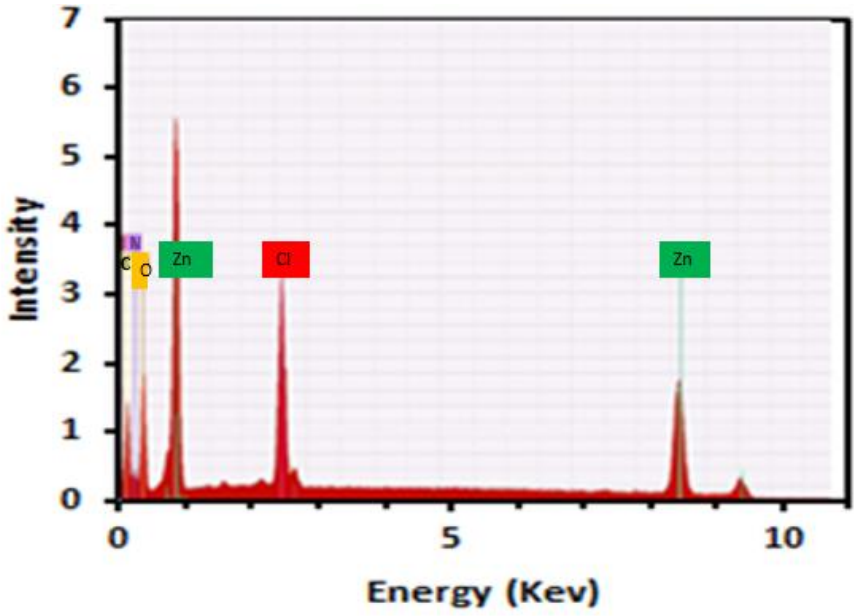

Figure 10. EDX microanalysis spectrum obtained by the analysis of micrograph 9c.

Furthermore, Figure 10 presents the EDX microanalysis on the micrographs of Figure 9d. The EDX analysis reveals the characteristic peaks of Zinc, thus demonstrating that the deposits consist of Zinc. The presence of nitrogen (N), oxygen (O), and chlorine (Cl) peaks are surface impurities. They come from the solvent consisting of a mixture of choline chloride $(CH_3)_3NCH_2CH_2OH(Cl)$ and urea $(NH_2)_2CO$) at which they are found. The carbon signal (C) comes from the electrode substrate made of carbon. These experimental analysis results conform with the studies of El Fazazi et al. [27] in aqueous media and those of HE et al. [35] in ionic liquid media.

4. Conclusion

The present work consists of the electrodeposition of Zinc on a glassy carbon electrode in choline chloride -urea (ChCl-U) media. The electrochemical results demonstrate that the zinc salt is soluble in the choline chloride-urea media. The cyclic voltammetry measurements made it possible to highlight the transfer of two electrons by the presence of an anodic and cathodic peak linked to the redox reaction of the Zn (II)/Zn couple. The appearance of a loop in the voltammogram made it possible to highlight deposition kinetics controlled by nucleation and growth. Data from experimental curves of transient current density versus time show a typical three-dimensional (3D) mass transport controlled by nucleation and growth phenomenon with a diffusion coefficient of $1{,}9\times 10^{-6} cm^2.s^{-1}$.

This process occurs instantaneously according to the formalism of Scharifker and Hills. The current efficiency of 99.4% was found at 100°C with less power consumption in the temperature range of 70 to 110°C. The deposit's surface morphology study by scanning electron microscope shows that they are amorphous at 70°C, whereas between 100°C and 110°C, the deposits are very crystalline. EDX analysis reveals the characteristic peaks of Zinc highlighting deposits made up of Zinc. The presence of peaks of nitrogen (N), oxygen (O), and carbon (C) are surface impurities. The chlorine comes from the solvent.

References

1. F. Porter, Corrosion Resistance of Zinc and Zinc Alloys, Corrosion Technology, 1st Edition 1994, EBook Published **2014**. EBook ISBN 9780429080746. https://doi.org/10.1201/9781482293524.
2. Z. Liu, T. Cui, G. Pulletikurthi, A. Lahiri, F. Endres, A Prussian Blue/Zinc Secondary Battery with a Bio-Ionic Liquid-Water Mixture as Electrolyte, American Chemical Society Applied Materials and Interfaces, **2016**, 8, 12158-12164. https://doi.org/10.1021/acsami.6b01592.
3. J. Roylance, K-S. Choi, Electrochemical Reductive Biomass Conversion: Direct Conversion of 5-Hydroxymethylfurfural (HMF) to 2,5-Hexanedione (HD) via Reductive Ring-Opening, Green Chemistry, **2016**, 10, 2956-2960. https://doi.org/10.1039/C6GC00533K.
4. H. Liu, S. Szunerits, W. Xu, R. Boukherroub, Preparation of Superhydrophobic Coatings on Zinc as Effective Corrosion Barriers, American Chemical Society Applied Materials and Interfaces, **2009**, 1, 1150-1153. https://doi.org/10.1021/am900100q.
5. K. Maniam, S. Paul, Corrosion Performance of Electrodeposited Zinc and Zinc-Alloy, Coatings in Marine Environment Corrosion Material Degradation, **2021**, 2, 163-189. https://doi.org/10.3390/cmd2020010.
6. E. L. de Araújo, A. M. Rodrigues, A. B. Viana, R. B. Viana, The Influence of Glycerol as an Additive in Zinc-Manganese Alloy Coatings Formed by Electrodeposition, Acta Scientiarum Technology, **2019**, 41, E41103. ISSN online: 1807-8664. http://dx.doi.org/10.4025/actascitechnol.v41i1.41 10.
7. J. L. Ortiz-Aparicio, Y. Meas, G. Trejo, R. Ortega, T. W. Chapman, E. Chainet, Effects of Organic Additives on Zinc Electrodeposition from Alkaline Electrolytes, Journal of Applied Electrochemistry, **2013**, 43, 289-300. DOI: 10.1007/S10800-012-0518x.
8. Q. Rayée, T. Doneux, C. Buess-Herman, Underpotential Deposition of Silver on Gold from Deep Eutectic Electrolytes, Electrochimica Acta, **2017**, 237, 127-132. https://doi.org/10.1016/j.electacta.2017.03.182.
9. A. P. Abbott, G. Capper, D. L. Davies, R. K. Rasheed, V. Tambyrajah, Novel Solvent Properties of Choline Chloride/Urea Mixtures, Chemical Communications, **2003**, 1, 70-71. https://Doi.Org/10.1039/B210714G.
10. E. L. Smith, A. P. Abbott, K. S. Ryder, Deep Eutectic Solvents and Their Applications, Chemical Review, **2014**, 114, 11060-11082. Https://Doi.Org/10.1021/Cr300162p.'
11. F. Ilgen, D. Ott, D. Kralisch, C. Reil, A. Palmberger, B. König, Conversion of Carbohydrates into 5-Hydroxymethylfurfural in Highly Concentrated Low Melting Mixtures, Green Chemistry, **2009**, 11, 1948-1954. https://Doi.Org/10.1039/B917548M.'
12. R. Bomparola, S. Caporali, A. Lavacchi, U. Bardi, Silver Electrodeposition from Air and Water-Stable Ionic Liquid: An Environmentally Friendly Alternative to Cyanide Baths, Surface Coatings Technology, **2007**, 24, 9485-9490. Https://Doi.Org/10.1016/j.Surfcoat.2007.04.008'
13. A. P. Abbott, J.C. Barron, G. Frisch, S. Gurman, K. S. Ryder and A. F. Silva, Double Layer Effects on Metal Nucleation in Deep Eutectic Solvents, Phys. Chem. Chem. Phys,**2011**,13,10224–10231'.
14. L.Vieira, R.Schennach, B.Gollas, The Effect of the Electrode Material on the Electrodeposition

of Zinc from Deep Eutectic Solvents, Electrochimica Acta **2015**, http://Dx.Doi.Org/10.1016/j.Electacta.2015.11.030.
15. E. Emanuele, A. Li Bassi, A. Macrelli, C. Mele, J. Strada, B. Bozzini, Zinc Electrode Cycling in Deep Eutectic Solvent Electrolytes: An Electrochemical Study. Molecules 2023, 28, 957. https://Doi.Org/ 10.3390/Molecules28030957).
16. J. Chen, M. Zhu, M. Gan, X. Wang, C. Gu, J. Tu, Rapid Electrodeposition and Corrosion Behavior of Zn Coating from a Designed Deep Eutectic Solvent. Metals 2023, 13, 172. https://Doi.Org/ 10.3390/Met13010172.).
17. C. Xiao, X. Cunying, X. Qinqin, W. Shuxian, L. Jianru, H. Yixin, The Effect of the Zinc Salt on the Electrochemical Behaviors of Zn in ChCl-urea Deep Eutectic Solvent, Journal of Solid State Electrochemistry, Ionics 2023, 29 :1255–1265, https://Doi.Org/10.1007/S11581-023-04879-2).
18. X.L. Zhu, C.Y. Xu, J. Tang, Y.X. Hua, Q.B. Zhang, H. Liu, X. Wang, M.T. Huang, Selective Recovery of Zinc from Zinc Oxide Dust Using Choline Chloride Based Deep Eutectic Solvents, Transactions of. Nonferrous Metals Society,2019 29, 2222−2228.
19. Q. Xiang, · S. Wang, J. Li, Y. Hua, The Effect of the Zinc Salt on the Electrochemical Behaviors of Zn in ChCl-urea Deep Eutectic Solvent, Journal of Solid State Electrochemistry, Ionics 2023, 29 :1255–1265, ttps://Doi.Org/10.1007/S11581-023-04879-2.
20. H. Yang, R. Reddy, Electrochemical Deposition of Zinc from Zinc Oxide in 2 :1 Urea/Choline Chloride Ionic Liquid, Electrochimica Acta, 2014, 147, 513-519. https://Doi.Org/10.1016/j.Electacta.2014.09.137.
21. X. Xueliang, Z. Xingli, L. Xionggang, L. Changyuan, C. Hongwei, X. Qian, Z. Zhongfu, Electrodeposition of Zn and CuZn alloy from ZnO/CuO precursors in a deep eutectic solvent, Applied Surface Science, **2016** 385, 481-489. https://doi.org/10.1016/j.apsusc.(2016).05.138))
22. M. Harati, D. Love, W. Lau, Z. Ding, Preparation of Crystalline Zinc Oxide Films by One-Step Electrodeposition in Reline, Materials Letters, **2012**, 89, 339-342. http://dx.doi.org/10.1016/j.matlet.2012.08.136.
23. H. F. Alesary, S. Cihangir, A. D. Ballantyne, R. C. Harris, D. P. Weston, A. P. Abbott, K. S. Ryder, Influence of Additives on the Electrodeposition of Zinc from a Deep Eutectic Solvent, Electrochimica Acta, 2019, 304, 118-130. https://Doi.Org/10.1016/j.Electacta.2019.02.090.
24. S. Ganesan, P. Ganesan, B..N. Popov, Electrodeposition and Characterization of Zn-Mn Coatings for Corrosion Protection Surface & Coatings Technolog 238 (2014).143-151.
25. K. K. Maniam and S. Paul, Progress in Electrodeposition of Zinc and Zinc Nickel Alloys Using Ionic Liquids, Applied Sciences, **2020**, 10, 5321. Doi:10.3390/app10155321.
26. A. A. Ortiz Verdín, R. O. Borges, G. T. Cordova, Y. M. Vong, Electrodeposition of Ni-Rich Alloys from an Acidic Deposition Solution by a Normal Codeposition Mechanism, Electrochemical and Solid-State Letters, **2011**, 14, 72-75. http://dx.doi.org/10.1149/1.3567029.
27. A. El Fazazi, M. Ouakki, M. Cherkaoui, Electrochemical Deposition of Zinc on Mild Steel, Mediterranean Journal of Chemistry, **2019**, 8, 30-41. https://doi.org/10.13171/mjc8119021318mo.
28. D. Sylla, C. Savall, M. Gadouleau, C. Rebere, J. Creus, Ph. Refait, Electrodeposition of Zn–Mn Alloys in Acidic and Alkaline Baths. Influence of Additives on the Morphological and Structural Properties, Journal of Applied Electrochemistry, **2005**, 200, 2137-2145. https://doi.org/10.1016/j.surfcoat.2004.11.020.
29. G. Deng, Q. Zeng, J. Huang, Electrodeposition Behaviors of Zn-Ni Alloy on Copper Foil with Carrier, 5th International Conference on Advanced Engineering Materials and Technology, **2015**, 423-428. http://dx.doi.org/10.2991/icaemt-15.2015.83.
30. A. Redjechta, K. Loucif, L. Mentar, M. R. Khelladi, A. Beniaiche, Electrodeposition and Characterization of Cu-Zn Alloy Films Obtained from a Sulfate Bath, Materials and Technologies, 2014, 48, 221-226. ISSN 1580-294.
31. J. B. Bajat, V. B. Mišković-Stanković, J. P. Popić, D. M. Dražić, Adhesion Characteristics and Corrosion Stability of Epoxy Coatings Electrodeposited on Phosphate Hot-Dip Galvanized Steel, Journal of Serbian Chemical Society, 2008, 63, 201-208. https://Doi.Org/10.1016/j.Porgcoat.2008.06.002.
32. Po-Yu Chen, M.-C. Lin, I-W. Sun, Electrodeposition of Cu-Zn Alloy from a Lewis Acidic ZnCl2-EMIC Molten Salt, Journal of The Electrochemical Society, **2000**, 147, 3350-3355. https://doi.org/10.1149/1.1393905.
33. Y. Wang, H. Yeh, Y.Tang, C. Kao, P. Chen, Voltammetric Study and Electrodeposition of Zinc in Hydrophobic Room-Temperature Ionic Liquid 1-Butyl-1-Methylpyrrolidinium Bis((Trifluoromethyl)Sulfonyl) Imide ([BMP][TFSI]): A Comparison between Chloride and TFSI Salts of Zinc, Journal of The Electrochemical Society, 2017, 164, 39-47. https://Doi.Org/10.1149/2.0451702JES.'
34. A. Maciej, N. Łatanik, M. Sowa, I. Matuła, W. Simka, Electrodeposition of Copper and Brass Coatings with Olive-Like Structure, Chemistry and Materials Science, **2021**, 14, 1762-1765. https://doi.org/10.3390/ma14071762.
35. W. He, L. Shen, Z. Shi, B. Gao, X. Hu, J. Xu, Z. Wang, Zinc Electrodeposition from Zinc Oxidein the Urea/1-Ethyl-3-Methylimidazolium Chloride at 353 K, Electrochemistry-Tokyo, 2016, 84,

872-877.
http://Dx.Doi.Org/10.5796/Electrochemistry.84.872.
36. J. C. Myland, K. B. Oldham, Cottrell's Equation Revisited: An Intuitive, but Unreliable, Novel Approach to the Tracking of Electrochemical Diffusion, Electrochemical Communication, **2004**, 6, 344-350. https://doi.org/10.1016/j.elecom.2004.01.013.
37. L. Simanavicius, A. Stakenas, A Sarkis, the Initial Stages of Aluminum and Zinc Electrodeposition from an Aluminum Electrolyte Containing Quaternary Aralkylammonium Compound, Electrochimica Acta, **1997**, 42, 1581-1586. https://doi.org/10.1016/S0013-4686(96)00319-2.
38. J. Depoorter, X. Yan, B. Zhang, G. Sudre, A. Charlot, E. Fleury and J. Bernard, All Poly(Ionic Liquid) Block Copolymer Nanoparticles from Antagonistic Isomeric Macromolecular Blocks via Aqueous RAFT Polymerization-Induced Self-Assembly, Polymer Chemistry, **2021**, 12, 82-91. https://doi.org/10.1039/D0PY00698J.
39. B. Scharifker, G. Hills, Theoretical and Experimental Studies of Multiple Nucleation, Electrochemical Acta, **1983**, 28, 879-889. https://doi.org/10.1016/0013-4686(83)85163-9.
40. B. Scharifker, J. Mostany, Three-Dimensional Nucleation with Diffusion Controlled Growth, Journal of Electroanalytical Chemistry Interfacial Electrochemistry, **1984**, 177, 13-23. https://doi.org/10.1016/0022-0728(84)80207-7.
41. M. S. Rehbach, J.H.O.J. Wijenberg, E. Bosco, J. H. Sluyters, The Theory of Chronoamperometry for the Investigation of Electrocrystallisation Mathematical Description and Analysis in the Case of Diffusion-Controlled Growth, Journal of Electroanalytical Chemistry, **1987**, 236, 1-20. https://doi.org/10.1016/0022-0728(87)88014-2.
42. L. Heerman, A. Tarallo, Theory of the Chronoamperometric Transient for Electrochemical Nucleation with Diffusion-Controlled Growth, Journal of Electroanalytical Chemistry, **1999**, 470, 70-76. https://doi.org/10.1016/S0022-0728(99)00221-1.
43. P. Allongue, E. Souteyrand, Metal Electrodeposition on Semiconductors: Part 2. Description of the Nucleation Processes, Journal of Electroanalytical Chemistry, 1993,362, 79-87. https://Doi.Org/10.1016/0022-0728(93)80008-6.